

Control of the temporal shape of nanosecond long lasers using feedback loops

Contact: pedro.oliveira@stfc.ac.uk

P. Oliveira, S. Addis, J. Gay, K. Ertel, M. Galimberti and I. Musgrave

Central Laser Facility, STFC Rutherford Appleton Laboratory, Harwell Campus, Didcot OX11 0QX, UK

Abstract

We present developments in the control of the temporal pulse shape of nanosecond long pulsed lasers. An active feedback loop between the output of a regenerative amplifier and its input to obtain the desired pulse shape is demonstrated. Several algorithms to achieve this, and the differences due to the targeted pulse shape and duration, are compared in this paper. It is found that the algorithm that is based on the ratio of the target and measured pulse profiles provides the most robust solution. The method proposed here can be used to obtain any pulse shape with minimal knowledge of the laser amplification system.

1 Introduction

The need to control the temporal profile of nanosecond long laser pulses is important for a wide range of experiments conducted on Vulcan. Unlike femtosecond lasers which have been widely studied [1], the temporal profile of nanosecond lasers can be controlled electronically. Temporal resolutions of 100s of picoseconds can be obtained using conventional electronics to shape the pulse, by means of Pockels cells [2, 3], or directly modulate laser diodes by controlling their current [4], or using an optical fibre-based low voltage electro-optic modulator (EOM).

We have been able to control the temporal profile at the output of a regenerative amplifier (RGA) by controlling the temporal profile of the seed laser. The seed pulse is generated using an EOM and an arbitrary waveform generator (AWG). To generate the required temporal profile, some authors [3, 5, 6] have calculated pulse temporal deformations due to saturation using simulations and/or analytical models. These models rely on the value of the saturation fluence and the small signal gain remaining constant. However, these models assume static conditions and cannot easily accommodate other temporal effects or day-to-day changes. Therefore, we have developed a feedback system that enables the output pulse to be maintained even if the other parameters change.

To demonstrate this we have used an RGA in which the pulse propagates 50 passes within the amplifier; furthermore, both the Pockels cell (PC) inside the RGA and the external contrast PC have a temporally non-uniform transmission. In addition to the square pulse distortion expected in saturated amplifiers, the pulse overlaps in the gain medium; this creates an additional temporal feature as shown in Figure 1.

Figure 1 shows an initially 5 ns top-hat pulse (yellow) that is amplified in the RGA: the feature at 3.5 ns (blue) is due to the pulse overlap in the gain medium. Lastly, on a long term time scale, slight misalignments will change the saturation in the RGA.

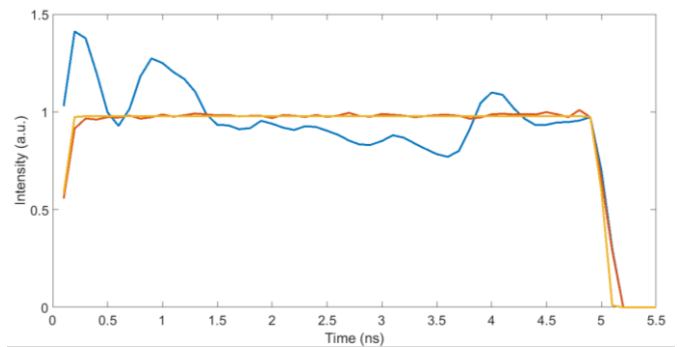


Figure 1: Deformation of the pulse temporal profile due to our RGA system. We input a 5 ns top hat temporal profile in into our system (in yellow) and get the blue waveform at the output. After the described corrections we obtain the waveform in red.

In this paper, we present the results for three feedback algorithms: one that simply uses the difference between the temporal profile of the seed pulse and the output pulse; a second one that uses the same idea but with an adaptive proportionality constant; and a third one that uses the ratio of the two temporal profiles. We investigated top hat, exponential and ramp pulse shapes for durations of 1, 3 and 5 ns. We start by presenting the architecture of our system and explain how we match and calibrate the relative time bases of our measurement system and the AWG control (Section 2). In Section 3, we present our experimental parameters: the target pulse shapes and the algorithms that were tried, and give details of how we analyze them in Section 4. Subsequently we present our results in Section 5.

2 Architecture of our ns RGA laser system

The architecture of our system is as follows. A continuous-wave (CW) (100mW) laser is sliced using a modulator (LiNbO₃ EOM, NIR-MX-LN-10 ixblue). These pulses are then injected into an RGA cavity, where the pulse is amplified to the mJ level. At the output of the RGA, a Pockels cell (CPC) is added in order to improve the contrast of the laser pulse, after which the pulse is further amplified in an amplifier chain. At the output of this system we have a fibre-coupled photodiode (PD, DET08CFC/M) connected to a 12.5 GHz oscilloscope (DPO71254C). The oscilloscope communicates with our CPU via an Ethernet connection. The voltage applied to the EOM is controlled by an AWG, which in turn is controlled using a serial port connection to our CPU (Figure 2).

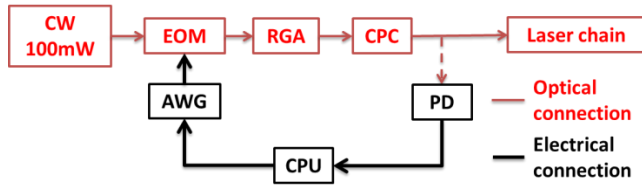


Figure 2: The architecture used in our study

The relation between the transmission of the EOM and the AWG output voltage, V_{AWG} , is defined by a sine square function (as given by the supplier datasheet). Controlling this transmission allows us to control the intensity of the seed. The AWG used during this experiment has a temporal window of up to 30 ns comprising individual Gaussian pulses that are spaced a nominal 100 ps apart. The voltage of each individual pulse can be set between 0 and 5 V. In order to calibrate the time scale between the control in the AWG and the measurement in the oscilloscope, we generated a picket fence pulse shape with a spacing of 10 samples. The voltage on this picket fence is the maximum transmission voltage ($\frac{\pi}{2}$ voltage). We detected the peaks of this picket fence (shown in Figure 3) and, from this, made a linear adjustment between the detected peak times on the oscilloscope and the defined peaks in the AWG.

The temporal profile measured by the detection system is the convolution of the actual pulse profile and the impulse response of the detection system. To determine the impulse response of the system, we used a 3 ps and a 10 ps laser pulse to determine that it has a FWHM of 142 ps. We then fitted a Gaussian curve to the impulse response and used this as a low pass filter. It is this low pass filtered waveform that we used as our target waveform, as shown in Figure 4.

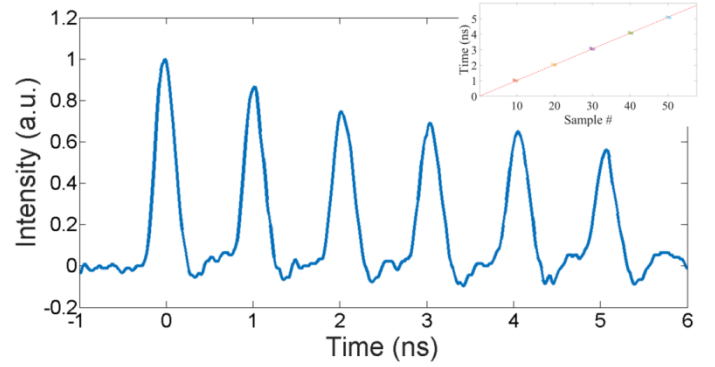


Figure 3: The picket fence as acquired by the oscilloscope. In this instance the timing between samples was 102 ps (top-right) Linear relation between the sample number and the time stamp

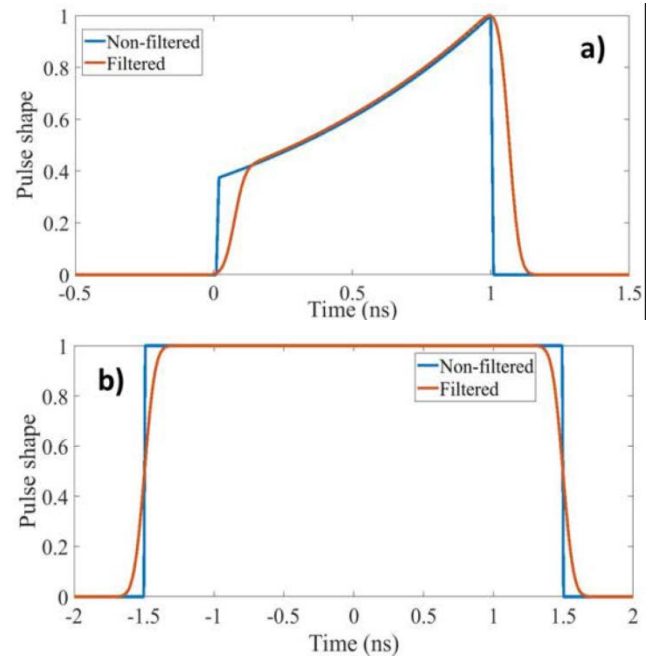


Figure 4: Target pulse profiles before and after the use of the instantaneous response, a) 1 ns exponential, and b) a 3 ns top hat.

3 Methods and experimental parameters

To study the feedback algorithms under test, we scanned for differences in the pulse duration, and several types of pulse shapes. We used an exponential pulse shape with 1 ns, 3 ns and 5 ns pulse duration. The non-filtered exponentials will be determined by the equation: $T(t) = \exp(t/C)$, where $T(t)$ is the target waveform in which C is chosen so that the exponential goes from 0.4 of the maximum to the maximum within the pulse duration (blue line in Figure 4). We also studied a 1 ns and 5 ns top hat shape: in these cases, the rise time of the AWG was important (200 ps). In addition, we used a ramp profile which went from 0 to maximum in 5 ns.

3.1 Algorithms used to correct the pulse shape

We analyzed four possible algorithms; all of the feedback loops compare the pulse profile obtained at the output of the previous loop, $R_{n-1}(t)$, to the target profile, $T(t)$, and then modify the input seed profile, $S_{n-1}(t)$, to determine the next seed pulse profile to apply, $S_n(t)$. For all these algorithms we started by inputting the desired waveform (non-filtered) as a first guess. The result of this input begins the feedback loop. The first algorithm (Eq. (1)) is based on the difference between the target profile $T(t)$ and the obtained pulse profile on the last iteration, where P is a variable set in the feedback loop.

$$S_n(t) = S_{n-1}(t) + P(T(t) - R_{n-1}(t)) \quad (1)$$

The second algorithm uses the same relation as that expressed in Eq.(1), but the proportionality constant is dependent on the error obtained on the previous iteration, ϵ_{n-1} (defined in Eq.(5)). After some trials, we decided to try a non-linear expression in which we would have a certain maximum P defined as the initial error and a decrease in P with a decrease in error. The term ϵ_0 in Eq. (2) is the error given on the first trial.

$$P_n(t) = P_{max} \left[1 - \left(\frac{\epsilon_{n-1}}{\epsilon_0} - 1 \right) \right] \quad (2)$$

The third algorithm is based on the ratio between the target and the obtained waveform.

$$S_n(t) = S_n \left(P \left(\frac{T(t)}{R_{n-1}} - 1 \right) - 1 \right) \quad (3)$$

We explored a fourth algorithm. Similarly to the first algorithm, we used the difference between the result of the previous and the target shape to obtain the seed of the following iteration. In this algorithm, however, we also used the results from previous iterations and the difference between the target and the result, as expressed in Eq. (4).

$$S_{n+1}(t) = S_n(t) + P(T(t) - R_n(t)) + I \frac{1}{n} \sum_n (T(t) - R_n(t)) \quad (4)$$

This last algorithm has two parameters to scan, so we only applied it to the 3 ns exponential. We did not find any value of I in Eq. (4) that improved the speed or precision of the algorithm and so we do not present the results of this investigation in this paper. In all algorithms after using Eqs. (1) to (3) the seed pulse profile was renormalized. This allowed the maximum voltage on the AWG to be equal to the half-wave voltage of the modulator. We scanned the parameter P for algorithms 1 and 3, and P_{max} in algorithm 2, for values from 0 to 1 in 0.1 steps, and

for each parameter we did 28 iterations.

4 Data Analysis

In this section we describe the methods used to consistently analyze more than 5,600 pulse shapes.

4.1 Definition of error and nonlinear error

As we want to compare different pulse shapes, there is a risk that quantizing the normalization of these pulse shapes is an ambiguous procedure. To minimize this risk, we chose an error definition based on a standardized second momentum (Eq.(5)). This definition: minimizes the error; does not depend on normalization of the result; does not depend on normalization of the target; and does not depend on the number of points used to calculate the error and hence on the pulse duration. This is a slightly different version of what is used in ultrafast pulses [1]. We represent each point of the targeted shape as $T(t)$ and of the result as $R(t)$.

$$\epsilon = \sqrt{\frac{\sum(T(t) - \gamma R(t))^2}{\sum T(t)^2}} \quad (5)$$

where:

$$\gamma = \frac{\sum(T(t)R(t))}{\sum R(t)^2} \quad (6)$$

Because this measurement is taken *ad hoc*, some local anomalies might not be detected. It is necessary to go further and define an error that highlights local anomalies. To achieve this, we define a nonlinear error given by Eq. (7)

$$\epsilon_{NL} = \sqrt[10]{\frac{\sum(T(t) - \gamma R(t))^{10}}{\sum T(t)^{10}}} \quad (7)$$

Each time we determined the resulting pulse shape we use an average of 10 sequential acquisitions to minimize random static error.

4.2 Convergence and error analysis

The characteristic result is a reduction of the error and a convergence of the temporal profile to our target; we show this in Figure 5. In this figure, we illustrate how the error between the target and output profile reduces as function of the number of iterations.

By fitting an exponential fit to the error as a function of the iteration number we can evaluate the speed of convergence, base error and whether the error converged or not (Eq.(8)).

$$F = A \exp(-S_n) - D_n + \epsilon_B \quad (8)$$

F is the fitting function; n is the iteration number; S is a measurement of the speed (to be more precise it is the number of iterations that it takes for the

variation in error to decrease by e^{-1} of the maximum variation); E_B is the base of the curve; and D is a measurement of the divergence. Fitting this curve provides us with a systematic and a quantitative analysis of the results that is not sensitive to transient numerical fluctuations.

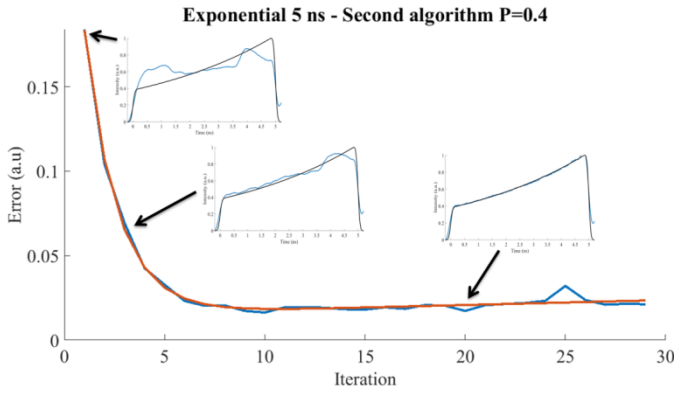


Figure 5: Error decrease with the iteration number (blue curve) using a 5 ns exponential waveform and the curve fitted to this (red curve)

5 Results

In Figures 6 to 11 we present the results for the speed of convergence, and the minimum obtained error for each of the pulse shapes, for each of the algorithms and for each of the P parameters. For those data sets where the exponential fit to the decrease of the error was not adequate, the speed does not appear in the plots; however, we still plot the minimum error obtained at each loop trial, even if there was no point in calculating the speed of the decrease.

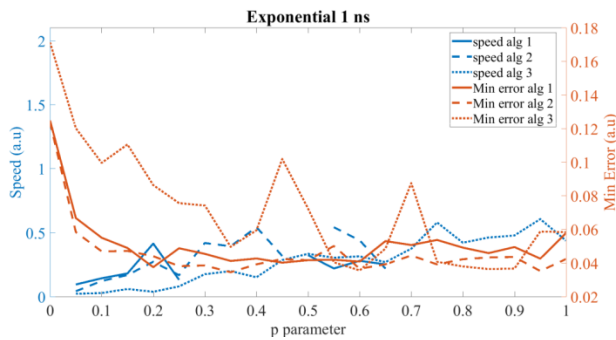


Figure 6: Speed and minimum error for a 1 ns exponential function

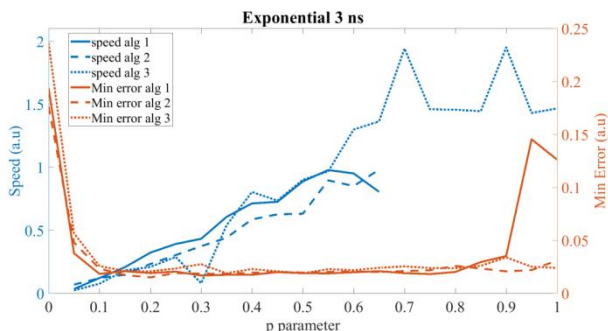


Figure 7: Speed and minimum error for a 3 ns exponential

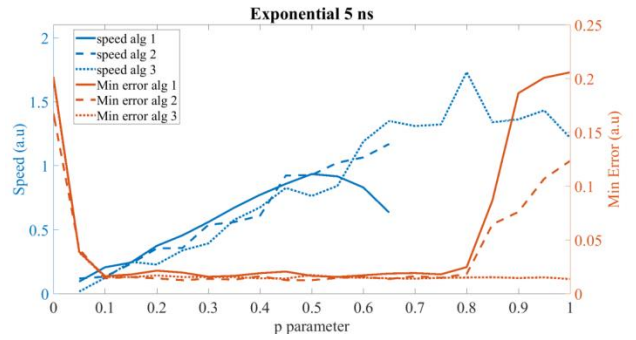


Figure 8: Speed and minimum error for a 5 ns exponential

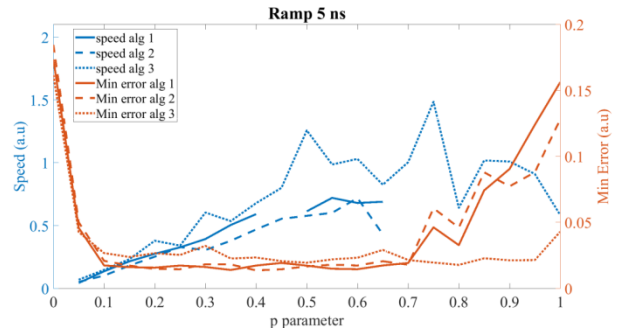


Figure 9: Speed and minimum error for a 5 ns ramp curve

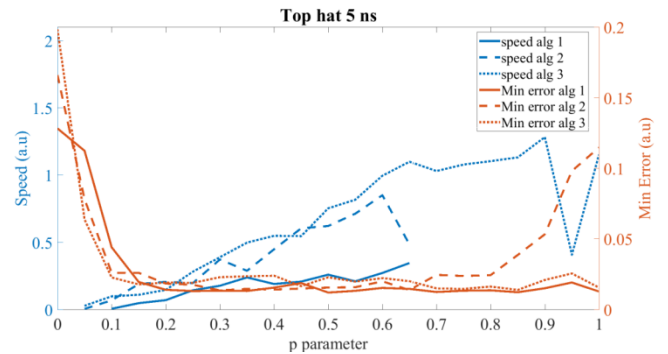


Figure 10: Speed and minimum error for a 5 ns top hat pulse

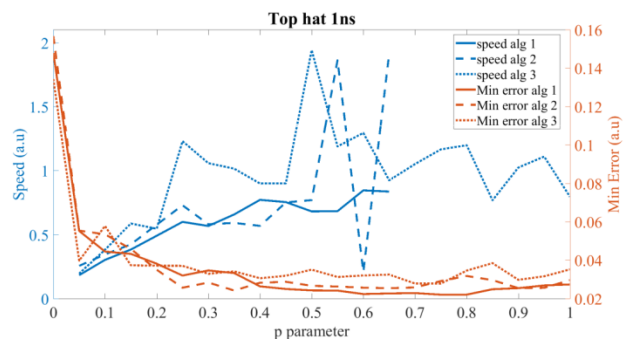


Figure 11: Speed and minimum error for a 1 ns top hat pulse.

6 Discussion

For the first and second algorithms, the behaviour is only exponential for $P < 0.7$. Algorithm 1 is more unstable because it fails for some values of P smaller than 0.65. Algorithm 3 works for every value of P .

For all algorithms, as the value of parameter P increased, the speed of convergence increased. In fact, except for 5 ns top hat profiles, we can also say that for a certain value of P all the algorithms have the same speed: this means that algorithm 3 can converge more quickly than the other algorithms, because it can operate at higher values of P .

For the 5 ns top hat profile, it is shown that the speed of algorithm 1 is about 50% of what we observe for the other pulse shapes. For this same shape and duration, algorithms 2 and 3 have a speed reduced by 30% in comparison with other pulse shapes, which is easily explainable because, in this pulse shape, the front of the pulse has more influence over what happens on the back of the pulse than other pulse shapes.

Comparing the same pulse shape but different pulse durations we observe that for 1 ns pulse duration a speed that is smaller than for longer pulse durations (by approximately 50%).

When considering all P values, we seem to be able to obtain the same error for 3 ns and 5 ns no matter the algorithm used; however, for algorithm 3 the same minimum error was only obtained for P values bigger than 0.7.

The error between 1 ns pulses and 3 ns pulses characteristically decreased by a factor of two (from 0.04 to 0.02), but between 3 ns and 5 ns the decrease was negligible (0.02 to 0.018).

For the same pulse duration, the differences in the minimum obtained error between the several shapes that we tried (top hat, ramp and exponential) were negligible.

7 Conclusion

In this paper, we have presented a method to correct the temporal pulse profile at the output of a regenerative amplifier by changing the seed pulse using a feedback loop. This method considers the instantaneous response and matches the relative timescales of the seed and the output. This method is applied simply using knowledge of the input and the output of the system, without any simulation of the amplifier itself or the elements in it.

The analysis of the results is based on an exponential decrease of the error as a function of the number of iterations. The error was defined to be independent of pulse duration, shape and the normalization of the target and the result temporal profile.

We have presented results on three algorithms that can be used for this effect, two in which the correction is based on the difference between the target profile and the profile obtained for a certain seed, and a third that is based on the ratio of both profiles.

We observed a significant difference in terms of accuracy between pulses of 1 ns and 3 ns, but negligible difference between 3 ns and 5 ns. This might be because the response time of both the seed system and the measuring system is on the order of 150 ps.

In order to maximize the accuracy of the shape and the speed of the algorithm, the proportionality factor P should be within the range 0.5-0.65 for the first two algorithms, whereas a parameter value within the range of 0.7-0.9 is optimal for the third algorithm.

For both algorithms 1 and 2, the values of P that make the algorithm stable but lead to higher values of speed are between 0.5-0.65. We conclude by saying that the method that minimizes the error and presents the biggest speed of convergence is algorithm 3 with P values in the range 0.7 to 0.9.

References

- [1] *Trebino R., 'Frequency Resolved Optical Gating', Springer (2000)*
- [2] *Friedman W., Seka W., Soures J., 'On the generation of temporally shaped laser pulses for inertial confinement', Optics Communications **25**, 103 (1978)*
- [3] *Xu L., Yu L., Chu Y., Gan Z., Liang X., 'Temporal compensation method of pulse distortion in saturated laser amplifiers', Applied Optics **54**, 357 (2015)*
- [4] *Vu K.T., Malinowski A., Richardson D.J., Ghiringhelli F., Hickey L.M.B., Zervas M.N., 'Adaptive pulse shape control in a diode-seeded nanosecond fiber MOPA system', Optics Express **14**, 10996 (2006)*
- [5] *Schimpf D.N., Ruchert C., Nodop D., Limpert J., Tu"nnermann A., Salin F., 'Compensation of pulse-distortion in saturated laser amplifiers', Optics Express **16**, 17637 (2008)*
- [6] *Malinowski A., Vu K.T., Chen K.K., Nilsson J., Jeong Y., Alam S., Lin D., Richardson D.J., 'High power pulse fiber MOPA system incorporating electro-optic modulator based adaptive pulse shaping', Optics Express **17**, 20927 (2009)*